Preprint
UCRL-JC-138876

Thermal Explosion Violence of HMX-Based Explosives – Effect of Composition, Confinement and Phase Transition Using the Scaled Thermal Explosion Experiment

J.L. Maienschein, J.F. Wardell, J.E. Reaugh

U.S. Department of Energy

Lawrence Livermore National Laboratory

This article was submitted to JANNAF CS/APS/PSHS Joint Meeting, Monterey, CA, November 13-17, 2000

October 25, 2000

This work was performed under the auspices of the United States Department of Energy by the University of California, Lawrence Livermore National Laboratory under contract No. W-7405-Eng-48.

THERMAL EXPLOSION VIOLENCE OF HMX-BASED EXPLOSIVES – EFFECT OF COMPOSITION, CONFINEMENT AND PHASE TRANSITION USING THE SCALED THERMAL EXPLOSION EXPERIMENT

J.L. Maienschein, J.F. Wardell, J.E. Reaugh
Lawrence Livermore National Laboratory
Livermore, CA

ABSTRACT

We developed the Scaled Thermal Explosion Experiment (STEX) to provide a database of reaction violence from thermal explosion of explosives of interest. A cylinder of explosive, 1, 2 or 4 inches in diameter, is confined in a steel cylinder with heavy end caps, and heated under controlled conditions until it explodes. Reaction violence is quantified by micropower radar measurement of the cylinder wall velocity, and by strain gauge data at reaction onset. Here we describe the test concept and design, show that the conditions are well understood, and present initial data with HMX-based explosives. The HMX results show that an explosive with high binder content yields less-violent reactions that an explosive with low binder content, and that the HMX phase at the time of explosion plays a key role in reaction violence.

INTRODUCTION

To understand the hazards involved in thermal explosions of energetic materials exposed to high temperatures such as fires, key considerations are the time to explosion and the violence of the ensuing reaction. Knowledge of these factors is important in developing strategies for fire fighting. Currently, we can predict with reasonable accuracy the time and temperature at which an explosion will take place, if the necessary information is available. This information includes thermal properties (specific heat, thermal conductivity, thermal expansion) and reaction kinetics (developed from small-scale experiments such as the One Dimensional Time to Explosion test[1]) for the explosive, thermal boundary conditions for the event, and details on the construction of the system. Clearly the accuracy of the prediction increases as more detailed kinetic and thermal data become available, but the methodology of this prediction is well established. Many simulation codes are available which have the necessary treatment of heat flow and chemical reactions to address the time of explosion.

Our ability to predict violence of the thermal explosion, which may range from a mild burn to a near-detonative explosion, is much more limited. The chemical and physical phenomena involved are very complex and not well understood. Unlike prediction of time to explosion, it is difficult to even enumerate the list of parameters that must be known to achieve a prediction. Computer simulations are much more difficult when violence is to be calculated, and only a few simulation codes exist which can realistically handle this problem. Despite these difficulties, efforts are underway at several laboratories aimed at prediction of violence of thermal explosion. At LLNL the simulation code ALE3D is being developed to address this type of problem.[2]

One limitation on reaction violence studies has been the lack of quantitative data on the violence of thermal explosions in past experiments. To be useful in developing predictive capability, and particularly in developing predictive simulation codes, experiments must measure the reaction violence under experimental conditions that are well characterized. Most thermal explosion experiments done to date in the Department of Energy and Department of Defense have been screening tests to determine qualitative violence, typically by observing number and size of fragments, or else have been of very small scale. Screening experiments are generally low-cost, so it is difficult to tightly control the external and internal conditions. Small scale experiments can be carefully designed to emphasize a particular aspect

Approved for public release, distribution is unlimited. Work performed under the auspices of the U.S. Department of Energy by Lawrence Livermore National Laboratory under contract No. W-7405-ENG-48.

of thermal reaction, but are difficult to extrapolate to scales more representative of actual systems. Recent experiments have taken a more quantitative approach

We developed the Scaled Thermal Explosion Experiment (STEX) to address the lack of quantitative data on thermal reaction violence. Here we describe the concept and design of the experiment, and report initial results with HMX-based explosives. Our goal is for this test to provide a database of violence of thermal explosions for materials of interest under well-controlled conditions, to support the development of a predictive capability for thermal explosion violence.

EXPERIMENTAL DESCRIPTION

CONCEPT

The STEX test was developed with the following goals: uniform heating for well-defined boundary condition; well-defined physical confinement; pre-determined reaction location away from end effects; a range of physical scales; quantitative measurements of reaction violence; and design to allow accurate simulations of the system, avoiding physical features that are difficult to model. To this end, we devised a cylindrical test where the reaction initiates in the axially-central region of the cylinder (radial location depends on heating rate). Confinement is provided by a steel wall and end caps with known mechanical properties that are insensitive to temperature. Confinement levels are 7.5, 15, or 30 ksi (50, 100, 200 MPa) set by selecting the thickness of the cylinder wall. We use three cylinder diameters, 1, 2, and 4 inch (25.4, 50.8, and 101.6 mm), with a constant length:diameter ratio of 4:1. Violence is quantified through non-contact micropower impulse radar as well as through strain gauges attached to the cylinder walls.

DESIGN

The design of the STEX vessel is shown in Figure 1. The cylindrical vessel is 4130 steel hardened to Rockwell 32C. A flange is brazed onto each end of the vessel, and sealed with a end cap using a metal O-ring and several heavy bolts. Dimensions are given in Table 1. The metal O-ring, from Parker-Hannifin Corporation, is a hollow torus made from X750 Inconel with a free height diameter of 0.125 in (3.2 mm), a wall thickness of 0.020 in (0.51 mm), and an overall diameter scaled to fit the diameter of the vessel and end flanges. The O-ring is internally vented so that internal pressure assists in achieving a leak-free seal at high pressures. In developing this design, we extensively analyzed the mechanical response of the system to anticipated stresses and ensured that the weak point in the system was the cylinder wall and not the end caps.

External temperature is controlled by three RTDs (one for cylindrical vessel and one for each end cap), and monitored by twelve additional RTDs placed at locations at 60° intervals 1/4, 1/2, and 3/4 of the way up the vessel; the RTDs are calibrated to ± 0.1°C. An internal thermocouple sheath is placed on the axis of the cylinder, in the explosive, with thermocouples at each end of the vessel and at 1/4, 1/2, and 3/4 height locations. The sheath is fabricated from type 304 stainless steel (0.0625 in OD, 0.016 in wall thickness) with a welded end plug; the sheath was designed to withstand 30 ksi (200 MPa) pressure, which is the maximum it should see before the final explosion. Type K thermocouples calibrated to ± 0.5°C are inserted into the sheath to measure the temperature at the positions given above. Strain gauges to monitor hoop and axial strain are located on the external cylinder wall, two configured for hoop strain and two for axial strain. The experimental configuration is shown in Figure 2, which shows the three radiant heaters used to heat the cylinder wall. These non-contact heaters, positioned 5.5 in (140 mm) from the vessel wall, were chosen to reduce temperature gradients that are typically present with heater bands, and to eliminate the non-quantifiable extra confinement that heater bands provide. The three heaters are controlled by one temperature controller monitoring a RTD that is located at the center of the vessel between two of the heaters. Each end cap is heated with a separately-controlled heating element.

The location of the three radar transmitting and receiving horns is also shown in Figure 2; these are placed 7 in (178 mm) from the vessel wall in the spaces between heaters. By using three radar channels we measure wall velocity at three angular locations around the vessel. The micropower impulse radar sends out short pulses of microwave radiation and measures the time to return; each channel has a

different sequence of pulses, allowing discrimination of each channel and eliminating cross-talk between channels.[3] We chose micropower radar for wall velocity measurement because of the long duration of these experiments and the unpredictability of the reaction time. More conventional wall velocity measurement methods using laser velocimetry are impractical due to difficulties with running a high-power laser for the several days of the experiment and then triggering the data acquisition system, in addition to problems posed by the significant heat load on the experiment from the laser. Flash radiography has been used successfully elsewhere to capture wall motion in this type of experiment – however, the resolution is poor (typically two flash images) and generally looks across only one plane of the experiment. Micropower impulse radar avoids these problems while providing a good measure of wall velocity.

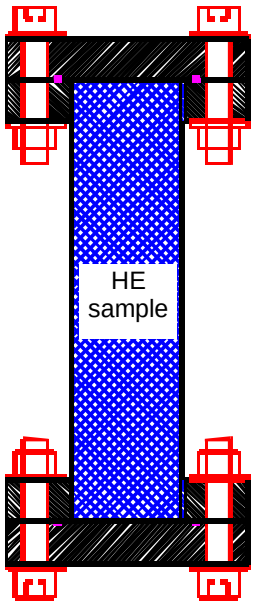

Figure 1. Design of STEX vessel. Dimensions are Table 1.

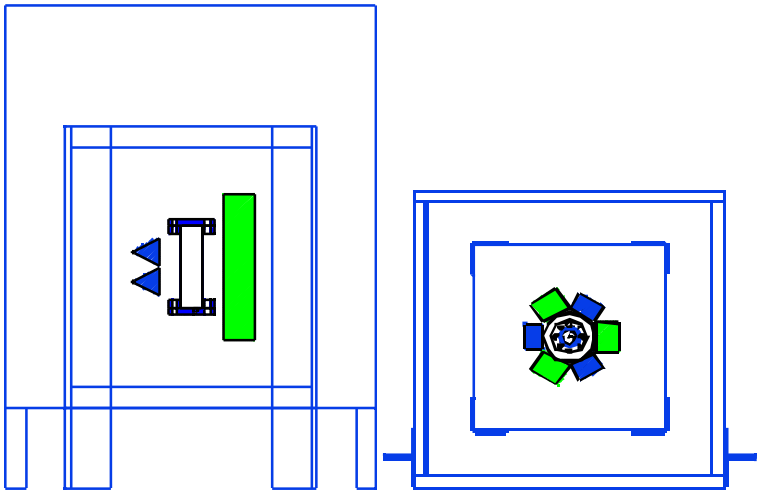

Figure 2. Layout of STEX experiment, side view (left) and top view (right), showing radar horns and radiant heaters. Small square on right is shot stand, and large square is shrapnel shield.

EXPERIMENTAL CONDITIONS

Calculations with chemical kinetic schemes for HMX-based explosives[1] showed that a heating rate of 1°C/hr was required to locate the ignition point at the center of a 2-inch diameter sample. At a rate of 1.44°C/hr, the calculated ignition point was about 0.4 inch (10 mm) from the edge. Because we expected maximum violence with center-ignited reactions, the experiments run to date have been heated at 1°C/hr from 130°C until thermal explosion occurs; ramp rates of 5 - 10°C/hr are used to heat to 130°C, chosen for experimental convenience, followed by a 5-hour soak at 130°C. The top and bottom flanges are set to lag the cylinder temperature by about 5°C, to ensure that the ignition location is centered along the axis of the cylinder.

The mass of explosive must be carefully chosen to allow for thermal expansion and the $\beta \rightarrow \delta$ phase transition in HMX, which is discussed in more detail below. Depending on desired conditions, the explosive can be sized to come in contact with the cylinder wall before or after the phase transition; for experiments with 30 ksi (200 MPa) confinement, the phase transition can be impeded by sizing the explosive so it comes snug before the transition can occur.

Table 1. Dimensions of STEX explosives vessel

Vessel inner diameter, length	1 inch (25.4 mm), 4 inch (101.6 mm)	2 inch (50.8 mm), 8 inch (203.2 mm)	4 inch (101.6 mm), 16 inch (406.4 mm)
Wall thickness:			
7.5 ksi (50 MPa)	0.020 inch (0.51 mm)	0.040 inch (1.02 mm)	0.080 inch (2.03 mm)
15 ksi (100 MPa)	0.040 inch (1.02 mm)	0.080 inch (2.03 mm)	0.160 inch (4.06 mm)
30 ksi (200 MPa)	0.080 inch (2.03 mm)	0.160 inch (4.06 mm)	0.320 inch (8.13 mm)
Flange thickness	TBD	1.00 inch (25.4 mm)	TBD
End cap diameter	TBD	6.00 inch (152 mm)	TBD
End cap thickness	TBD	1.12 inch (28.4 mm)	TBD

RESULTS AND DISCUSSION

CHARACTERIZATION OF EXPERIMENTAL SETUP

To ensure that the experimental conditions are well known, we tested components of the system separately. The cylindrical vessel was designed to rupture at 7.5, 15 or 30 ksi (50, 100, or 200 MPa). We tested one 30-ksi vessel to failure; the vessel was mostly filled with a Teflon insert, and then was pressurized with helium over a 30-minute span until it burst. This vessel burst at 24 ksi (166 MPa), and ruptured in the cylinder wall as expected. The burst pressure was somewhat lower than the design pressure, presumably the result of imperfect material properties; the failure point was in the cylinder and not in the end caps, as desired to ensure that the radar monitors the failure point of the vessel.

We tested the uniformity of the heating system by heating a 30-ksi vessel that contained a Teflon insert equipped with thermocouples placed against the inside of the wall at several heights and at six angular locations; we monitored the external RTDs and internal temperatures during a slow thermal ramp. At the vertical midpoint of the vessel, the external RTDs directly under the lamps had a spread of 0.7 ± 0.3°C, showing uniform heating from all three lamps. The external RTDs between the heaters had a smaller spread of 0.3 ± 0.2°C, again quite uniform. The external RTDs directly under the lamps read 2.4 ± 0.3°C higher than those between the lamps. As expected, heat transfer through the wall smoothed out the thermal profile at the inside of the cylinder wall; temperatures directly under the lamps were indistinguishable from those between the lamps. The angular temperature uniformity is therefore quite good. There is a deliberately-imposed vertical temperature gradient, achieved by controlling the lower end cap 5°C and upper end cap 9°C below the set point of the radiant lamps, to have the highest temperature in the center of the sample.

We tested the response of the micropower radar by measuring the wall velocity of a steel cylinder filled with 13-micron ammonium perchlorate at a density of 1.06 g/cm^3. Cylinder dimensions were 2 in (50.8 mm) inner diameter, 0.5 in (12.7 mm) wall thickness, 12 in long (305 mm). The cylinder was end-initiated with a P-22 plane wave lens, and the wall velocity about 2/3 of the way up was measured with radar and Fabry Perot velocimetry. Radar transmitting and receiving horns were placed 1 meter from the cylinder. The wall velocity was measured by radar as 820 fps (250 m/s), in good agreement (within 11%) with the velocity from Fabry Perot of 920 fps (280 m/s). We selected the low-density AP fill for this test shot anticipating that most thermal explosions would be relatively mild and therefore give low wall velocities. As will be seen below, some thermal explosions give wall velocities well in excess of 3300 fps (1000 m/s). The radar requires ~25 μs for one spatial sweep; therefore for a fragment traveling 2 feet (0.6 m) at a velocity of 3300 fps, the radar will record only about 25 distance-time points, and for higher velocities the resolution is still poorer. At low wall velocities (below 1000 fps or 300 m/s), the accuracy of the radar should be about 10% (consistent with the AP cylinder shot), but at higher velocities the accuracy is reduced to perhaps 20-25% at the highest velocities of 6600 fps (2000 m/s).

RESULTS WITH HMX-BASED EXPLOSIVES

We have studied two HMX-based explosives using the STEX test. LX-04 contains 85% HMX of trimodal particle size distribution and few large particles (> 100 μm), and 15% Viton A binder. PBX-9501 contains 95% HMX with a trimodal particle size distribution and a significant fraction > 100 μm, with a binder of 2.5% Estane and 2.5% BDNPA/F. Samples for most runs were uniaxially pressed to a density of > 98.5% of theoretical maximum, although samples for runs 1, 3, 6, 7 were pressed isostatically to about the same density. The key differences between these two formulations are the proportion of HMX to binder, and the presence of larger particles in the PBX-9501. We have conducted STEX tests at 7.5 and 30 ksi (50 and 200 MPa). Results from these tests are summarized in Table 2. One of the conditions in Table 2 is the solid phase of HMX at the time of explosion. The $\beta \rightarrow \delta$ phase transition involves a volumetric expansion of about 6% and therefore the phase transition is hindered by high pressure.[4-8] An approximate phase diagram for HMX is shown in Figure 3, based on literature data.[9-12] From this diagram, confining HMX at 30 ksi (200 MPa) increases the phase transition temperature by over 30°C. Therefore, by sizing the explosive sample so that it comes snug with the vessel wall before the phase transition, experiments with 30 ksi confinement can be conducted under conditions that prevent the phase transition; in this way, we can study the effect of HMX solid phase on thermal explosion violence. To illustrate the differences required, we can compare the sample sizes for PBX-9501 in runs 8 (δ-phase) and 11 (β-phase). For run 8 the PBX-9501 was 1.955 in (49.66 mm) diameter, 7.819 in (198.6 mm) long, 706 g; for run 11 the PBX-9501 was 1.9955 in (50.69 mm) diameter, 7.981 in (202.7 mm) long, 750 g. For each test, three cylindrical pieces of explosive were stacked to achieve the final height, with the center piece being approximately twice the length of the top and bottom piece; this was designed to ensure that the ignition point at the vertical center of the sample is not at a joint between two pieces.

Table 2. Summary of scaled thermal explosion experiments with HMX-based explosives. All are 2-inch diameter, 8-inch length (50.8 mm diameter, 203 mm length). All had a ramp rate of 1°C/hr above 130°C. Onset temperature is the highest reading on the vessel exterior at the time of runaway reaction. Some vessels leaked prior to thermal explosion, as shown by strain gauge and temperature data and by visual and aural observation. Violence is indicated by fragment distribution and by peak wall velocities measured by radar.

Test #	Explosive	Confinement, ksi (MPa)	HMX phase	Onset temp., °C	Leaked?	Fragments†	Wall velocity (3 channels), m/s
1	LX-04	3.8* (25)	δ	174	no	None	13, 0, 0
3	LX-04	7.5 (50)	δ	174	no	None	0, 0, 40
6	LX-04	30 (200)	δ	192	yes	4L, 4S	300, 600, 800
9	LX-04	30 (200)	δ	194	no	None	0, 800, 0
7	LX-04	30 (200)	β	187	yes	1 S	70, 0, 1000
10	LX-04	30 (200)	β	188	no	none**	N/A
2	PBX-9501	7.5 (50)	δ	170	no	none††	130, 60***, 130
4	PBX-9501	30 (200)	δ	169	yes	5 L, 9 S	600, 800, 200
8	PBX-9501	30 (200)	δ	170	no	6 L, 10 S	300, 800, 700
5	PBX-9501	30 (200)	β	168	yes	"Detonation"	1700, 1600, 1900
11	PBX-9501	30 (200)	β	167	no	"Detonation"	1400, 1700, 1200

* vessel was 7.5 ksi design, but had flaw in metal allowing failure at lower pressure.
† none – vessel split open; L: large fragments several inches in largest dimension; S: small fragments ~ 1 inch; "detonation" – vessel destroyed, hole punched in end cap, nothing recoverable from cylinder wall;
** Bottom heater failed during run. Reaction initiated above center of vessel, which split into three vertical segments aligned with three radiant heaters.
†† vessel completely split and folded back onto itself.
*** radar 2 recorded motion ~ 2ms later than radars 1 & 3, as the vessel walls folded back into view of radar 2.

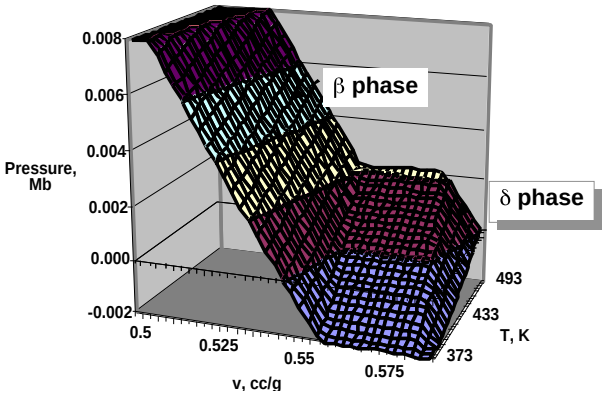

Figure 3. Approximate phase diagram for pure HMX, calculated from literature data.[9-12] The phase transition temperature increases with increasing pressure.

The violence of reaction may be evaluated two ways from the data in Table 2. First, the fragment pattern gives a qualitative sense, with violence ranging from simple vessel rupture with no fragmentation (runs 1, 2, 3, 9, 10), to rupture with one high speed fragment (run 7), to violent explosion with many fragments (runs 4, 6, 8) and finally to near-detonative reaction (runs 5, 11). Visual inspection of the experimental remains corroborates the different nature of the near-detonative reactions; the other runs have much of the experimental fixturing bent but still recognizable in place, while the near-detonative reactions reduce all components to small pieces and punch 2-inch diameter holes in the inch-thick end caps (Figure 4).

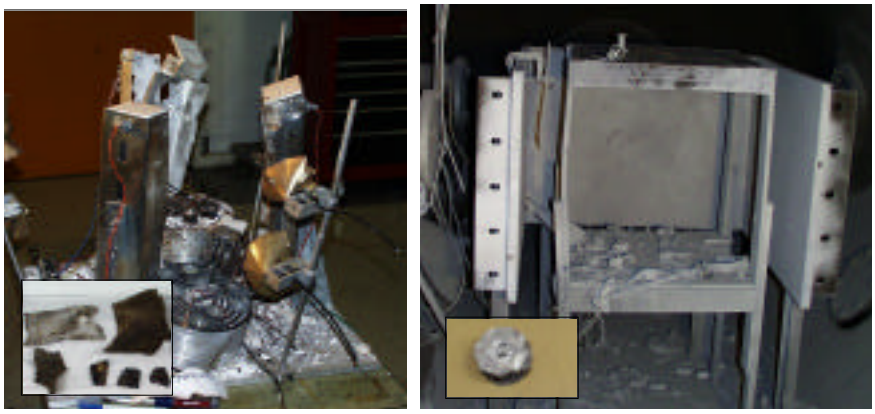

Figure 4. Left - remains of run 8, Table 2 - violent reaction. Radar horns and heaters are largely intact. Inset shows some fragments; smallest are about one inch across. Right - remains of Run 11, Table 2 - near-detonative reaction. All apparatus is reduced to tiny rubble. Inset shows 2-inch plug punched from one end cap.

The wall velocity data from the micropower radar are in good agreement with the qualitative observations from fragmentation. For experiments with no fragmentation, wall velocities are low and highly variable (run 9 showed a maximum velocity of 800 m/s, unusually rapid for no fragmentation, but two radar units detected no motion). The run that produced one fragment (run 7) apparently ejected it

towards one of the radar units, so this unit saw the small fragment moving rapidly while the other two radar units saw little-to-no motion. The runs with extensive fragmentation (runs 4, 6, 8) showed rapid wall motion on all radar units. The presence of large and small fragments may be interpreted as the large fragments coming from the region where reaction began, while the small fragments occurred where the reaction was well underway. This is consistent with the radar data for these runs, where the motion in one radar unit (on the side where the reaction initiated) is well below the velocity seen by the other channels, where the reaction had built up more intensity. In many cases we could match positions of fragments to radar channels, and in these cases the large fragments were associated with the low-velocity channel. Finally, the runs with a near-detonative reaction (runs 5, 11) showed very high velocities on all three radar channels, as could be expected from these fully-developed reactions; measured velocities range from 1200 – 1900 m/s. The wall velocities for these two runs should be considered lower estimates, because at the high velocities there are only a few points in the data set and aliasing can result in underestimation of the actual velocity. For comparison, the wall velocity from detonating PBX-9501 can be estimated using the Gurney model.[13, 14] For our configuration the velocity estimate ranges from 1900 – 2400 m/s, depending on how early the cylinder wall fractures. For the hardened steel in this experiment, early fracture is expected and a velocity of 1900 – 2000 m/s is a reasonable estimate. This is consistent with the velocities seen by the radar in the two near-detonative runs.

From the previous discussion, the data from the micropower radar are consistent with qualitative observation. But more importantly, the wall velocities provide a quantifiable measure of reaction violence that can be used to evaluate predictions for these explosives under these conditions. Furthermore, further analysis of the radar data can show additional details. For example, in run 2 the vessel ruptured in one location and folded back onto itself, as shown by the post-test debris. This was also seen in the radar data. One channel was aimed directly at the region of the vessel opposite where the rupture began, while the other two were aimed at the rupture region at about 60° angles - the two channels observing the rupture recorded very similar velocity profiles, while the channel aimed at the other side saw much lower velocities with a significant delay before any motion was detected.

Temperature and strain data are shown below for two runs. Figure 5 shows internal temperatures and hoop strain for run 4,PBX-9501 in 30 ksi (200 MPa) confinement. In the left plot, the phase conversion is visible in the internal temperature as the two endothermic features at 163-170°C. The presence of two endotherms can be attributed to the presence of large particles of HMX along with small particles in conjunction with the particle-size dependence of phase transition kinetics.[10, 11] The hoop strain shows a increase in this region as well, although it is more gradual since the strain is an volume-integrated measurement while the temperature measured is localized at the thermocouple. Also seen in the left figure is a perturbation close to the end of the experiment in both temperature and strain. This region is magnified in the right plot. The decrease in strain and temperature is the result of a leak through the internal thermocouple sheath, presumably near the sealed end of the sheath. The leak reduced the internal gas pressure and hence the strain. In addition, because the center of the sample was the hottest location in the test, the gas that passed through the thermocouple sheath when the leak occurred was cooler than the temperature being monitored by the internal thermocouple, and hence the temperatures also showed a decrease. Consistent with this explanation is the initial increase in temperature at the top and bottom, where the temperatures were apparently lower than that of the gas that passed through the sheath. Each of the first set of experiments (runs 4-7) with 30 ksi (200 MPa) confinement leaked in this manner; redesign of the thermocouple sheath eliminated this problem in the final four runs.

Figure 6 shows temperature and strain data for run 11, PBX-9501 in 30 ksi (200 MPa) confinement. Here the PBX-9501 was sized to come snug with the vessel prior to phase conversion, so that the phase conversion would be prevented. This experiment was also leak-free. The thermocouple and strain data show this, with no endothermic phase transition and no irregularities from leaks.

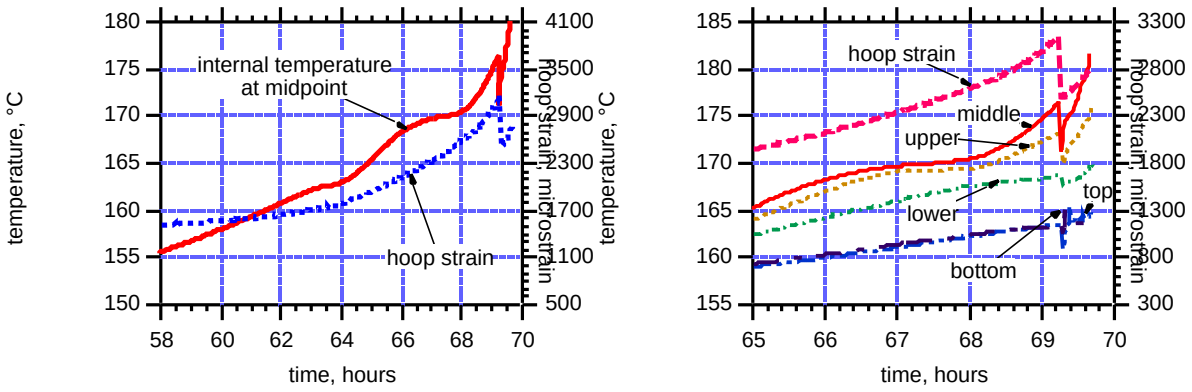

Figure 5. Temperature and strain data for run 4, PBX-9501 in 30 ksi (200 MPa) confinement. Left – internal temperature at center of vessel and hoop strain during heating, showing endothermic phase change in HMX. Right - internal temperature at the center of vessel and locations above and below center, and hoop strain; this plot is scaled to show the changes in temperature and strain when the vessel leaks.

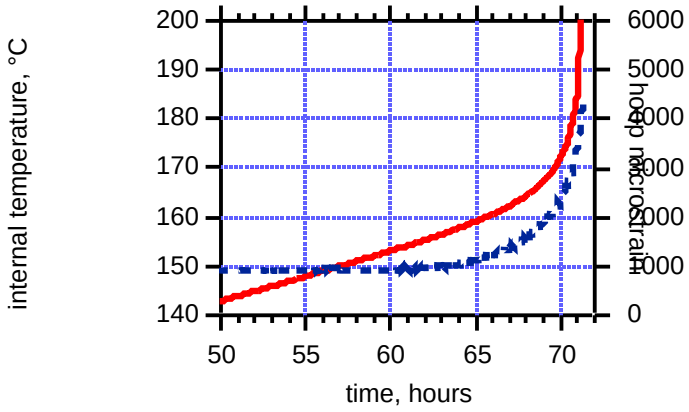

Figure 6. Temperature and strain data for run 11, PBX-9501 in 30 ksi (200 MPa) confinement; the sample was sized to maintain it in β-phase.

DISCUSSION OF HMX RESULTS

To date we have only conducted STEX tests with one thermal ramp rate and one size of confinement. Results are summarized in Table 2. The results thus far show that higher confinement leads to greater thermal explosion violence, as would be expected. With higher confinement, the reaction pressure is much higher before the apparatus disassembles explosively, and therefore the reaction rate and hence violence is greater.

The results also show that, under identical conditions, LX-04 gives reactions of lower violence than PBX-9501. Deflagration measurements with these materials at high pressures have shown that LX-04 has a constant pressure dependence up to pressures of 90 ksi (600 MPa), while PBX-9501 exhibits very rapid and erratic burning at pressures above 20 ksi (150 MPa).[15] This behavior was attributed physical deconsolidation of the explosive due to the low binder content and not the presence of large particles in the formulation, because a formulation that contained large particles in an LX-04 composition did not show deconsolidative burning. Because the buildup of deflagration ultimately leads to thermal explosion, it was expected that a low-binder formulation would give more violent thermal explosions, and this has been confirmed here.[15]

Results for runs designed to prevent the HMX phase transition are quite different for LX-04 and PBX-9501. With LX-04, the violence is not significantly affected by the HMX phase, whereas with PBX-9501 the violence changed character from a thermal explosion to a near-detonative reaction. There is some question whether the reaction was a true detonation, since the degree of metal flow on the end plugs was lower than some would expect. We will test this in the future by detonating a charge and observing the response of confinement and the velocities measured by radar. Regardless of whether the reaction is a true shock-driven detonation, the reaction violence is much greater for a heavily confined system where the HMX phase conversion is prevented.

Thermal explosion is preceded by a period where the interior of the explosive undergoes self-heating as the exothermic reaction accelerates. The onset of self heating is shown in Figure 7 for the runs at 30 ksi (200 MPa) confinement. We can make several observations from this plot. Overall, PBX-9501 begins to self-heat at a lower temperature than LX-04. The endothermic $\beta \rightarrow \delta$ phase change is clearly visible in the runs with LX-04 in δ phase, and is not seen in the runs with β phase HMX; the same is true for the runs with PBX-9501. For LX-04, the runs with β phase HMX reacted at lower external temperatures than with δ phase HMX, although this was not the case for PBX-9501. Finally, in all cases the runs where the seal was maintained showed self-heating of a shorter duration in comparison to the same run only vented. The most dramatic case was for PBX-9501 in the β phase, where in the sealed experiment there was very little self heating before explosion. This may be explained by the loss of gaseous intermediates and products in the vented case; energy is removed from the system both in the latent heat and the chemical energy in incompletely reacted species. The chemistry of the thermal explosion is therefore somewhat different in the vented and sealed cases. It is interesting to note that, despite these differences, the external temperature at the time of explosion, as shown in Figure 2, is essentially unchanged for vented and sealed systems.

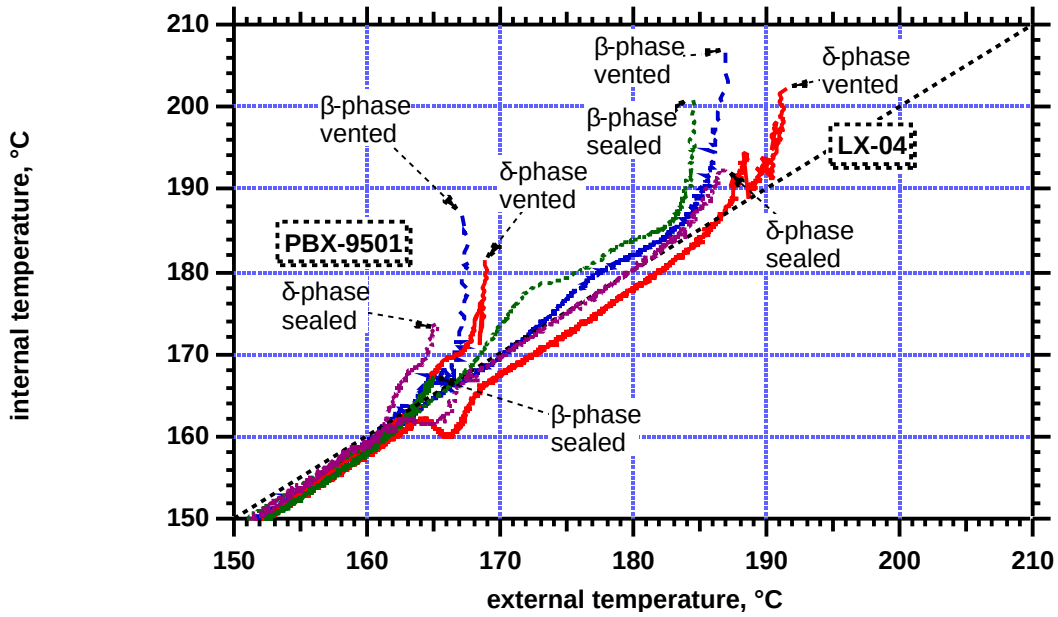

Figure 7. Self-heating data for each run at 30 ksi (200 MPa) confinement. Arrows point to end of data, at which point explosion occurred. Internal temperature was measured at the internal thermocouple location of highest temperature (middle in all cases except run 10, which was hottest at the upper thermocouple as a result of failure of the bottom heater). External temperature is the hottest external temperature at the corresponding vertical location.

FUTURE IMPROVEMENTS IN THE STEX TEST

Several refinements of the STEX test are planned or underway. These include fast recording of the internal temperature and external strain immediately before the runaway reaction, high-speed video recording of the explosion, and monitoring the internal gas pressure with a pressure transducer. We are testing the first three refinements currently. We have seen interesting indications of thermal explosion followed by extinguishment and subsequent re-ignition in the preliminary high-speed video recordings done thus far, but we have not perfected the technique or proven that this is what we are seeing. We have recorded rapid strain and temperature signals, but are still analyzing the data. We expect to implement the pressure transducer for internal pressure in the next few months.

CONCLUSIONS

The scaled thermal explosion experiment, as reported here, was designed to provide quantitative data on the violence of thermal explosions under well controlled conditions; such data are needed to develop, calibrate, and validate predictive capability for thermal explosions using simulation computer codes. The STEX experiment was designed with modeling in mind, with experimental conditions as well-defined as possible and in a form amenable to modeling. Temperature and strain data provide information during the heating process, and cylinder wall velocities resulting from the explosion provide a quantitative measure of the violence. We have run several experiments with HMX-based explosives, all at one size and one heating rate, and plan to explore a range of sizes and heating rates in future tests. From the tests done to date we have shown that explosive composition and confinement play a large role in reaction violence, and the β to δ phase transition in HMX is very important. We continue to develop the test, and anticipate testing other explosives in addition to the HMX work reported here.

ACKNOWLEDGEMENTS

We would like to thank the following people for their contributions. Al Nichols, Craig Tarver, LeRoy Green, Ed Lee, Matt McClelland, Ken Westerberg and Tri Tran have participated in the conceptual design and development of the STEX test as well as analysis of results. Electronic support has been provided by Dan Greenwood, Greg Sykora, Gary Steinhour and Don Burns. Mechanical and fabrication support has been provided by Les Calloway, Don Hansen, Barry Levine, Paul Marples, Brad Martin, Ken Montgomery, and Ed Silva. Tom Rosenbury, Doug Poland, Bob Simpson, George Governo and Aaron Jones have provided micropower impulse radar measurements. Rob Broderick, Bill Gilliam, Larry Crouch, Denise Grimsley, Pat McMaster, Ernie Urquidez, and Bob Gray have been very supportive in execution of these experiments in the High Explosives Applications Facility at LLNL.

REFERENCES

1. R.R. McGuire and C.M. Tarver, "Chemical Decomposition Models for the Thermal Explosion of Confined HMX, TATB, RDX, and TNT Explosives", in ***Proceedings of Seventh Symposium (International) on Detonation***, Annapolis, MD, Naval Surface Weapons Center, NSWC MP 82-334, p. 56 (1981).

2. A.L. Nichols, III, R. Couch, R.C. McCallen, I. Otero and R. Sharp, "Modeling Thermally Driven Energetic Response of High Explosive", in ***Proceedings of 11th International Detonation Symposium***, Snowmass, CO, Office of Naval Research, (1998).

3. E.T. Rosenbury, Lawrence Livermore National Laboratory, personal communication, March 1997.

4. H.H. Cady, "Studies on the Polymorphs of HMX", Los Alamos Scientific Laboratory, LAMS-2652 (October 18, 1961).

5. W.C. McCrone, "Crystallographic Data: Cyclotetramethylene Tetranitramine (HMX)", ***Analytical Chem.***, **22**, 1225 (1950).

6. A.S. Teetsov and W.C. McCrone, "The Microscopial Study of Polymorph Stability Diagrams", ***Microscop. Cryst. Front.***, **15**, 13 (1965).

7. M. Herrmann, W. Engel and N. Eisenreich, "Phase Transitions of HMX and their Significance for the Sensitivity of Explosives", in ***Proceedings of the Technical Meeting of Specialists*** MWD DEA AF-71-F/G-7304 - Physics of Explosives, p. 12 (1990).

8. R.E. Cobbledick and R.W.H. Small, "The Crystal Structure of the δ-form of 1, 3, 5, 6 - Tetranitro-1, 3, 5, 7-tetraazacyclooctane (d-HMX)", ***Acta Cryst.***, **B30**, 1918 (1974).

9. F. Goetz and T.B. Brill, "Laser Raman Spectra of α-, β-, γ, and δ-Octahydro-1,3,5,7-tetranitro-1,3,5,7-tetrazocine and Their Temperature Dependence", ***J. Phys. Chem.***, **83**, 340 (1979).

10. R.J. Karpowicz and T.B. Brill, "The β→δ Transformation of HMX: Its Thermal Analysis and Relationship to Propellants", ***AIAA Journal***, **20**, 1586 (1982).

11. R.J. Karpowicz, L.S. Gelfand and T.B. Brill, "Application of Solid-Phase Transition Kinetics to the Properties of HMX", ***AIAA Journal***, (1982).

12. A.G. Landers and T.B. Brill, "Pressure-Temperature Dependence of the β→δ Polymorph Interconversion in Octahydro-1,3,5,7-tetranitro-1,3,5,7-tetrazocine", ***J. Phys. Chem***, **84**, 3573 (1980).

13. B.M. Dobratz and P.C. Crawford, "LLNL Explosives Handbook: Properties of Chemical Explosives and Explosive Simulants", Lawrence Livermore National Laboratory, UCRL-52997 change 2 (January 31, 1985).

14. P.W. Cooper, ***Explosives Engineering***, VCH Publishers, New York, New York (1996).

15. J.L. Maienschein and J.B. Chandler, "Burn Rates of Pristine and Degraded Explosives at Elevated Pressures and Temperatures", in ***Proceedings of 11th International Detonation Symposium***, Snowmass, CO, Office of Naval Research, (1998).